Journal of the European Ceramic Society 45 (2025) 117162

Contents lists available at ScienceDirect

Journal of the European Ceramic Society

journal homepage: www.elsevier.com/locate/jeurceramsoc

Tailoring sintering properties of $BaGd_{0.3}La_{0.7}Co_2O_{6-\delta}$ steam electrodes for pressurized tubular proton-ceramic electrolysis cells

Laura Navarrete [a], Laura Almar [a], Mateusz Tarach [a], Einar Vøllestad [b], Asif Mahmood [c], David Catalán-Martínez [a], Sonia Escolástico [a], Marie-Laure Fontaine [b], Truls Norby [c], Jose M. Serra [a,*]

[a] Instituto de Tecnología Química (Universitat Politècnica de València – Consejo Superior de Investigaciones Científicas), Av. Los Naranjos, s/n, Valencia 46022, Spain
[b] SINTEF Industry, Sustainable Energy Technology, Forskningsveien 1, Oslo 0373, Norway
[c] Department of Chemistry, University of Oslo, Centre for Materials Science and Nanotechnology, Gaustadalleen 21, Oslo 0349, Norway

ARTICLE INFO

Keywords:
Proton ceramic
Electrode
Sintering aid
Barium zirconate
Electrolysis

ABSTRACT

We herein address manufacturing constraints related to the high-temperature sintering step required for reaching adequate adhesion of oxygen/steam electrodes on proton ceramic electrolytes, particularly in tubular geometry. Incorporating various sintering aids such as Cu, Co, and Ni oxides improves the sinterability of the electrodes and reduces the sintering temperature to 950 °C. The ceramic-ceramic composite electrodes based on $BaGd_{0.3}La_{0.7}Co_2O_{6-\delta}$ (BGLC37) and $BaZr_{0.7}Ce_{0.2}Y_{0.1}O_{6-\delta}$ (BZCY) show good and robust electrode-electrolyte adhesion. Composite electrodes were tested under different operation conditions, i.e., temperatures and oxygen partial pressures in symmetrical cell configuration, achieving apparent polarisation resistances below 0.6 $\Omega \cdot cm^2$ at 600 °C in wet air for all the electrodes with sintering aids. Finally, BGLC37/BZCY with 2 wt% of CuO electrodes were successfully applied on pre-reduced and sealed BZCY/Ni-supported tubular half-cells with 16 cm^2 active area and measured in electrolysis mode at 600 °C and high steam pressure. The results open a route to manufacturing steam electrodes for large-scale electrolysis cells.

1. Introduction

Proton Ceramic Electrolysis Cells (PCECs) employ proton (H^+) conducting electrolytes [1] to convert steam and electric power into H_2 more efficiently than conventional water electrolysis technologies. PCECs require, in principle, lower operation temperatures (below 600 °C) compared to Solid Oxide Electrolysis Cells (SOECs) since protons migrate with a lower migration barrier than oxide ions. Several studies have already demonstrated promising performance of PCECs operated at temperatures below 600 °C, employing $BaZr_{1-x-y}Ce_xY_yO_{3-\delta}$ (BZCY) or $BaZr_{1-x-2y}Ce_xY_yYb_yO_{3-\delta}$ (BZCYYb) as electrolyte [2,3] and Ni-BZCY cermet as negative electrode (cathode).

Dry and – depending on the configuration – electrochemically pressurised H_2 is generated at the cathode. In stack electrolyser design, planar and tubular geometries are the two primary choices. Planar geometry is the most predominant geometry for SOECs operating at ambient pressure reaching pre-commercial scale, while the planar PCEC technology is in comparison still in early stages of development. However, tubular cells are dominant in the upscaled production of PCECs to date. Proton ceramic tubular cells with active surface areas up to 60 cm^2, operating at high pressures (up to 10 bar) and under pressure gradients (up to 49 bar), have been tested without causing mechanical degradation or increasing the leakage rate across the cell [4].

The tubular technology offers superior mechanical tolerance to pressure and temperature fluctuations, and a smaller sealing area, which makes tubular PCECs preferable for pressurized operations and facilitate thermal management at stack level [5]. Currently, there are few public reports from projects to develop and address the challenges of tubular PCEC stack technology [6,7]. One of these – the European project GAMER – aimed to design and build tubular PCECs stacks for a 10 kW system operating at total pressures up to 30 bar. A simplified stack configuration was chosen as basis-of-design in this project, so-called "single tubular cell in shell" design, where a tubular electrochemical cell is encased in a steel pressure vessel, with necessary current collection, gas manifolds and current feedthroughs [7]. Each repeating unit integrates a tubular cell having an electrochemically active area of

* Corresponding author.
E-mail address: jmserra@itq.upv.es (J.M. Serra).

https://doi.org/10.1016/j.jeurceramsoc.2024.117162
Received 30 September 2024; Received in revised form 6 November 2024; Accepted 17 December 2024
Available online 18 December 2024
0955-2219/© 2024 The Authors. Published by Elsevier Ltd. This is an open access article under the CC BY-NC-ND license (http://creativecommons.org/licenses/by-nc-nd/4.0/).

60 cm^2 and consuming approximately 65 W. This requires a robust production of the repeating units to build up capacity, with an estimated 128 units required to achieve the desired system target. As documented in previous studies, the production of tubular half-cells is based on upscaled protocols integrating extrusion of the hydrogen electrode and spray-coating of the electrolyte, followed by co-sintering of the half-cells. Both green layers consist of the mixture of oxide and salt precursors, relying on solid state reactive sintering to produce the desired half-cells. Addition of the steam electrode, typically a composite of BZCY with an electronically conducting oxide with additional proton and oxide ion transport (triple conducting oxide) has been a critical and more challenging task [8]. Therein, the steam electrode is applied on a fully reduced and pre-sealed tubular half-cell requiring annealing in a dual atmosphere to ensure that the Ni-BZCY electrode is not oxidized during the thermal treatment. Other challenges are associated with potential delamination and spallation of the electrode layer due to mismatches in the thermal expansion of the functional layers and associated stresses during sintering and cooling processes.

Steam electrodes for PCECs require mixed protonic and electronic conductivity, and there has been significant effort over the last decade to develop catalytically active materials with favourable hydration thermodynamics [19–24]. Double perovskites, like cobaltites, are good steam electrode candidates in PCECs. For instance, $BaGd_{0.8}La_{0.2}Co_2O_{6-\delta}$ (BGLC82) exhibits low polarisation resistance [19,20,25,26] for PCECs, attributed to the ability to hydrate and hence incorporate protonic charge carriers in wet atmospheres [20]. These oxides typically exhibit large thermal expansion coefficient, well above $15–20{\cdot}10^{-6}\ K^{-1}$ in air, which has prone their use as a composite electrode with the electrolyte material to mitigate thermal expansion mismatch. [1,3,27,28]. Notwithstanding this, the mismatch in thermal and chemical expansion between these Co-containing perovskites and the refractory BZCY electrolyte material complicate the production of complete cells with clean interface, well adherent and nano-structured porous electrode.

High sintering temperatures (~1200 °C) and/or long dwell times are usually required to ensure good adhesion between the BGLC-BZCY composite electrode and the BZCY electrolyte, adversely affecting chemical structure (e.g. cation demixing of BGLC, loss of volatile elements), microstructure (grain growth, migration and segregation of phases) and porosity of the electrode, potentially damaging the electrode/electrolyte interface. An approach to reduce sintering temperature is to use sintering additives. For instance, the addition of small quantities of sintering additives in BZCY compounds has a beneficial effect on densification of this phase by reducing the sintering temperature from 1600 °C to 1450 °C [9,10]. In previous works, various sintering aids, like CuO, NiO [11,12], ZnO [13,14], SnO, MgO, or Al_2O_3[15], have been employed in doped barium cerates and zirconates and their solid solutions. Nevertheless, several reports also highlight that use of transition-metal oxides as sintering aids reduce the sintering temperature but adversely affects conduction properties. Park et al. [15] concluded that the effect of Cu on the bulk conductivity is insignificant, while it reduces grain boundary (GB) conductivity [16]. Similar results were obtained with ZnO on BZCY electrolytes [16,17] and BZY systems, showing segregation of cations in the grain boundaries [18]. High densification and larger grain size are obtained when NiO is incorporated in the BZCY, but it impacts on the hydration properties of the electrolyte materials and therefore its conductivity [11,12].

In this work, tailoring the manufacturing of steam electrodes on planar and tubular proton ceramic cells is envisaged by using sintering additives in the composite BGLC-BZCY electrodes and studying how this method can affect compatibility, adherence, and performance of the electrode, as well as of each individual phase. Electrodes with a 50/50 vol% mixture of BZCY and BGLC37 are fabricated in order to adjust the thermal expansion coefficient (TEC) between the electrolyte and the electrode. Various metal oxides are pre-selected as sintering aids, including CuO, NiO, and Co_3O_4, to enhance the sinterability of the composite electrode [29,30]. The optimized steam electrode with the most promising sintering aid (type and amount) is furthermore validated by further transfer of manufacturing in larger-scale tubular cells being electrochemically characterized under pressurized steam operating conditions.

2. Methodology

For the electrode architecture, commercial powder from Marion Technologies and Ceramic Powder Technology AS, $BaGd_{0.3}La_{0.7}Co_2O_{6-\delta}$ (BGLC37) and $BaZr_{0.7}Ce_{0.2}Y_{0.1}O_{6-\delta}$ (BZCY) were selected, respectively. BGLC37 and BZCY were mixed in 50 vol% and ball milled with zirconia balls in acetone for 16 hours.

To obtain a metal oxide loading of 2 and 5 wt% in the final BGLC37/BZCY-based electrodes, $Co(NO_3)_2{\cdot}6\ H_2O$, $Cu(NO_3)_2{\cdot}2.5\ H_2O$ or $Ni(NO_3)_2{\cdot}6\ H_2O$ were dissolved in different aqueous solutions. The BGLC37/BZCY mixture was impregnated by the incipient wetness method by dropping the different solutions on the powder. Then, the impregnated powder was dried and calcined at 600 °C (2 h) to ensure the formation of the different metal oxides (CuO, NiO, and Co_3O_4), ground, and sieved.

The $BaZr_{0.7}Ce_{0.2}Y_{0.1}O_{6-\delta}$ (BZCY) electrolytes were fabricated by milling the commercial powder with zirconia balls in acetone with 1 wt % ZnO. Dense BZCY electrolytes were prepared by uniaxial pressing and firing at 1565 °C for 12 h to densify the electrolyte disks fully.

Screen-printing inks made of BGLC37/BZCY with the different metal oxides and loadings were prepared by mixing in a three-roll mill; powders and a 6 wt% ethylcellulose-terpineol solution in a 1:1 wt ratio. The resulting pastes were screen printed on both sides of a ~0.75 mm-thick dense BZCY electrolyte (15 mm in diameter). Porous electrodes were obtained after calcining the resulting screen-printed layers at 950 °C for 12 h. A top screen-printed gold ink contact layer was applied to the electrodes to ensure proper current collection and sintered at 900 °C. X-ray diffraction (XRD) was carried out in a PANalytical Cubix fast diffractometer using CuKα1,2 radiation, with an X'Celerator detector and Bruker D8 in Bragg-Brentano geometry. XRD patterns were recorded in the 2θ range from 20 to 100° and analysed using the X'Pert HighScore Plus software.

The chemical compatibility between electrode and electrolyte infiltrated with 2 wt% or 5 wt% sintering aids (CuO, Co_3O_4, and NiO) were examined after thermal treatments using XRD. A mixture of BGLC37/BZCY with and without the addition of the sintering aids was sintered at 950 °C for 12 h. The chemical stability under pressurized electrolysis working conditions was studied at 600 °C for 100 h. Samples were treated at 4 barg of total pressure with a stream containing 50 % steam, 30 % Ar, and 20 % O_2.

Symmetrical cells were tested by Electrochemical Impedance Spectroscopy (EIS) using a Solartron 1470E/1455 FRA with an AC potential of 20 mV rms and a frequency sweep from 0.03 Hz to 1 MHz under open circuit conditions at temperatures from 650 to 500 °C in a humidified atmosphere (2.5 % H_2O), with different oxygen partial pressures (synthetic air and 1 % O_2). Post-mortem analysis of the symmetrical cells was done by Scanning Electron Microscopy (SEM) using a GeminiSEM 500 from Zeiss.

Complete tubular proton ceramic electrolysis cells were made using composite BGLC37/BZCY with 2 wt% CuO as the steam electrode. The composite electrodes were applied on sintered and pre-reduced Ni-BZCY/BZCY half-cells, which were already capped and sealed to an alumina riser (see reference [1] for details). The steam electrode was applied by dip-coating before the complete cell assembly was fired in a dual atmosphere (air on steam electrode, 30 % H_2 in Ar on fuel electrode) at 950 °C for 12 h. The electrode area was 16 cm^2. Ag paste and wire were used as a current collector system. The complete cell was mounted in a Probostat™ (NORECS AS, Norway) with a heated base unit, allowing operation with pressurised steam-containing steam atmospheres. The cell was operated at 600 °C and 4 barg total pressure on both compartments. During the measurements, the steam electrode was

fed with 50 % air and 50 % steam, while the hydrogen electrode was swept with 1.5 bar H_2, 0.25 bar H_2O, and 2.25 bar Ar.

3. Results

3.1. Electrodes compatibility and adhesion test

The chemical compatibility of the electrolyte and electrode materials (BZCY and BGLC37) was checked using XRD analysis after heat treatment of the powders mixture in order to reflect the thermal process history of the cell manufacturing. Fig. 1 shows the XRD patterns of the BGLC37 and BZCY mixtures prepared without sintering additive (Fig. 1 "None") and with 2 wt% or 5 wt% CuO, Co_3O_4 and NiO sintering aids (Fig. 1 2Cu, 5Cu, 2Co and 2Ni) after calcination at 950 °C for 12 h. All diffraction peaks can be assigned to the BZCY pattern (space group Pm-3m) and the BGLC37 pattern (space group P4/mmm), confirming the thermo-chemical compatibility of both phases. However, for samples infiltrated with CuO as a sintering aid, a peak split in the BGLC37 (space group P4/mmm) pattern related to a double perovskite structure can be identified, increasing with the concentration of CuO. Figure S1 shows that the cell parameters of BGLC37 and BZCY remain unchanged by sintering aids, indicating no doping into the crystal lattice.

The chemical stability under high steam content for the different electrodes prepared with sintering aids was evaluated by exposing the materials at 4.0 barg total pressure with a stream containing 50 % of steam, 30 % of Ar and 20 % of O_2 during 100 h (Fig. 2). All the samples had the same thermal history (950 °C 12 h) as the electrodes employed for the electrochemical cell measurements in the present work. X-ray diffraction analysis reveals that all samples retained their crystalline structure under the selected high steam content conditions. A small (less than 2 %) amount of $BaCoO_{2.93}$ is observed for all BGLC37/BZCY mixtures after steam treatment, being derived from the raw BGLC powder [1,31].

The prepared steam electrode inks (2Cu, 5Cu, 2Ni, 5Ni, 2Co, and 5Co) were first coated by screen printing on BZCY/Ni-supported tubular pre-reduced half-cells and sintered at 950 ºC to evaluate the attachment to the larger area tubular electrolytes prior the electrochemical characterization in button cells. The adhesion strength of the electrode to the electrolyte was verified by a 90º peeling test with a scotch tape. Details of the test procedure are provided in the Supplementary Information (Figure S2). All the electrode layers with 2 wt% sintering aid successfully passed the tape testing as well as the 5 wt% CuO. This strong and stable adhesion achieved for a low sintering temperature (950 °C) was not attainable for the same electrode compositions without sintering aids or with higher Co_3O_4 and NiO contents (5Co and 5Ni), which may be ascribed to lower CuO melting point (Figure S3).

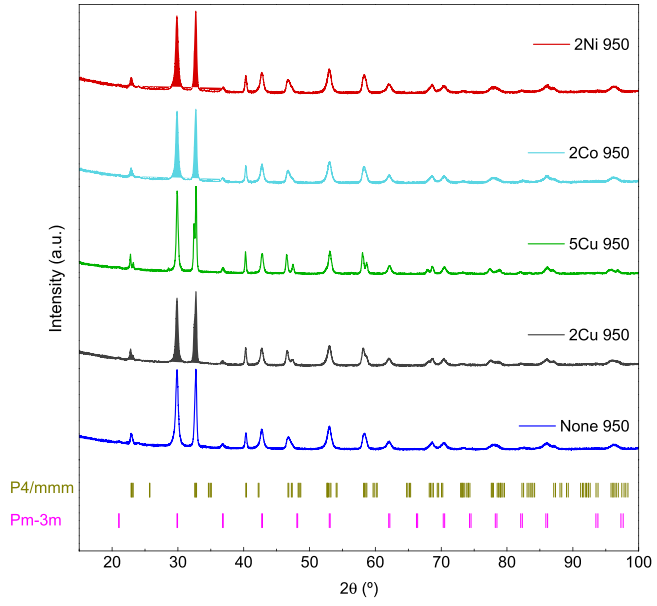

Fig. 1. XRD patterns of BGLC37/BZCY mixture (50 vol%) without and with sintering aids (2 wt% or 5 wt% CuO, Co_3O_4, and NiO) after being treated at 950 °C for 12 h.

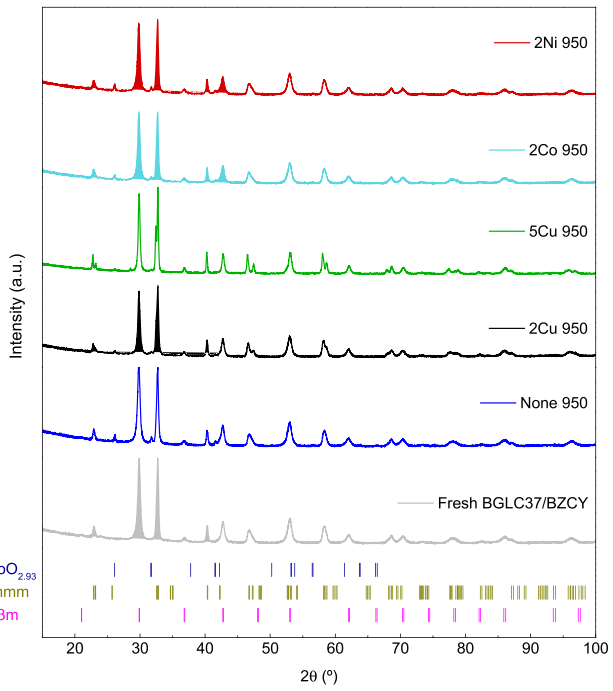

Fig. 2. High content steam stability: XRD patterns of BGLC37/BZCY without and with sintering aids (2 wt% or 5 wt% CuO, Co_3O_4, and NiO) after a treatment at 600 °C, 4 barg, and a stream composed by 50 % steam, 30 % Ar and 20 % O_2.

3.2. Electrochemical characterisation of composite steam electrodes

The electrochemical behaviour of the electrodes that showed good attachment to the tubular pre-reduced half-cells was checked in symmetrical disk-shaped cells (active area of 0.64 cm^2) of BZCY electrolytes in wet (2.5 % H_2O) oxidizing atmospheres as a function of temperature from 650 to 500 °C. Fig. 3 shows the polarisation resistance (Rp) of the different electrodes in an Arrhenius plot measured in wet air (a) and wet 1 % of O_2 (b). The polarization resistance values were obtained from the fitting of the EIS spectra using an equivalent circuit with three RQ-elements in series, i.e. $(R_{HF}CPE_{HF})(R_{MF}CPE_{MF})(R_{LF}CPE_{LF})$, since it was possible to distinguish three contributions in the high (> 1 kHz), mid (1000–1 Hz) and low (1–0.01 Hz) frequency ranges, HF, MF, and LF, respectively. In this study we only need qualitative and comparative electrode polarisation impedance data, and hence no measurements were made of electrolyte protonic, oxide ionic, and electronic partial conductivities or transport numbers, and the spectra were therefore not fitted with or corrected for a parallel electronic path in the electrolyte and not attempted to be split into two ionic rails from protons and oxide ions [20]. As a result, the apparent polarisation resistances reported here will be underestimated of the actual ones – especially as temperature increases – and apparent activation energies hence overestimated.

The total apparent Rp at 600 °C in humid air ranges between 0.4 and 0.6 Ω·cm^2 for the different electrode compositions, which is similar to that obtained for $BaGd_{0.8}La_{0.2}Co_2O_{6-\delta}$ single-phase electrodes [20]. Steam electrodes with Ni (2Ni) and Co (2Co) oxides as sintering aids exhibited the best performance under both oxygen contents, followed by

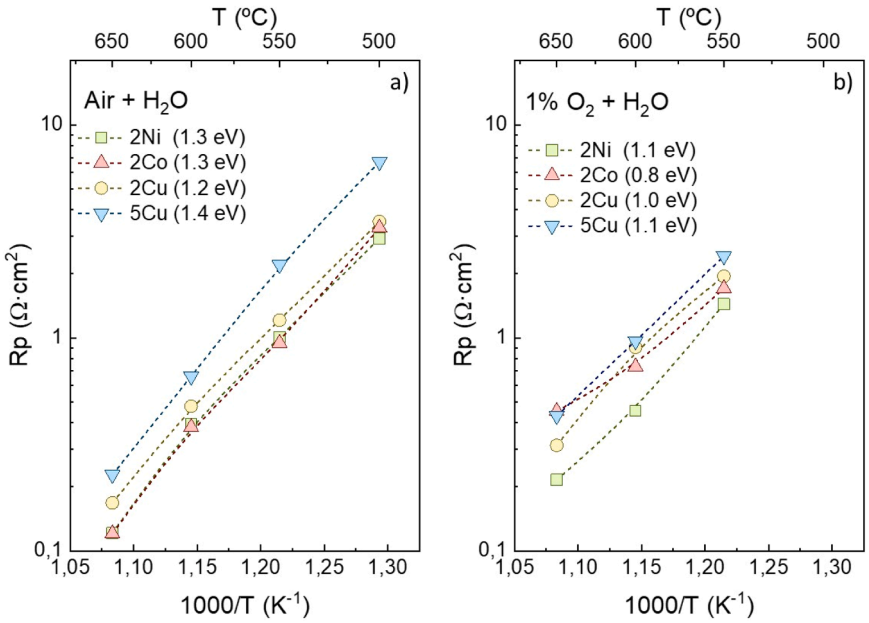

Fig. 3. Rp as a function of the temperature of different electrodes with sintering aids under humidified air (a) and humidified 1 % O_2 stream. The apparent activation energies (E_a) are presented in parentheses.

the electrode with 2 wt% CuO (2Cu). A higher content of CuO (5 wt% CuO) resulted in an increase of the polarization resistance that can be ascribed to higher sintering and shrinkage – in thickness – of the electrode, giving rise to an excess reduction of the electrode porosity, i.e., electrochemically-active surface area.

All the electrodes presented an apparent activation energy (E_a) ranging between 1.2 and 1.4 eV in wet air and decreasing to 0.9–1.1 eV in wet 1 % O_2. These values are similar to other state-of-the-art electrodes in humidified oxidising conditions for PCECs [20,32]. The larger activation energy observed in air can be attributed to the larger contribution from p-type electronic conductivity in the BZCY electrolyte, which reduces the apparent polarization resistances at the highest

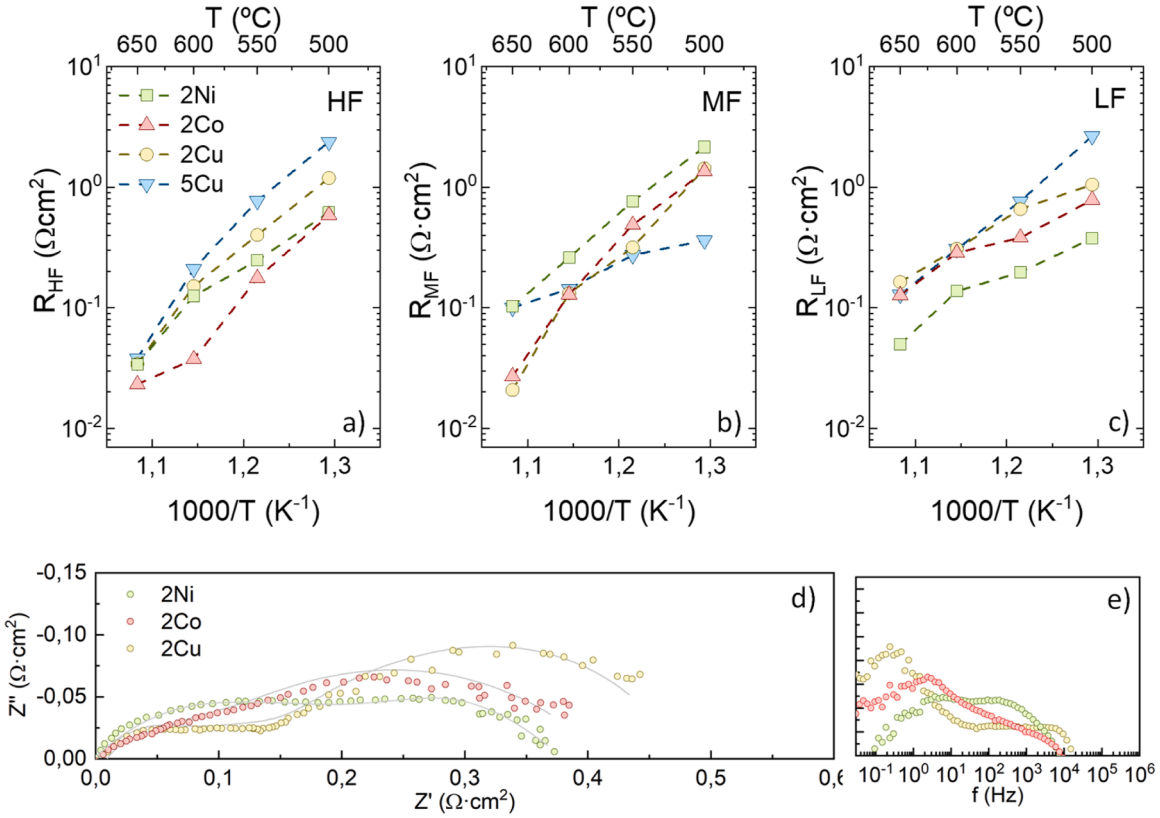

Fig. 4. HF (a), MF (b), and LF (c) resistances obtained from the equivalent circuits of the BGLC37/BZCY 2 wt% Co_3O_4, BGLC37/BZCY 2 wt% NiO, BGLC37/BZCY 2 wt% CuO and BGLC37/BZCY 5 wt% CuO electrodes measured in wet air. Nyquist (d) and Bode plots (e) at 600 ºC in wet air for 2Cu, 2Ni, and 2Co electrodes.

temperatures. Accordingly, the activation energies measured in 1 % O_2 more accurately depict the protonic processes at the electrode, in agreement with the behaviour previously observed for BGLC82 electrodes [20].

Fig. 4 shows the resistance contributions for the low, mid, and high-frequency ranges (R_{HF}, R_{MF}, and R_{LF}), respectively, fitted from the impedance spectra as a function of the temperature for the electrodes measured in wet air. The HF contribution has an associated pseudo-capacitance lower than 10^{-4} F·cm^{-2} which is typical for electrodes limited by the charge-transfer reaction [20,32]. Higher content of sintering aid (5 vs 2 wt% CuO) increases R_{HF}, which may be speculated to reflect a blocking resistance of CuO between electrode particles. The MF contribution is usually attributed to proton diffusion and/or surface reaction kinetics [20]. All the electrodes exhibited a pseudocapacitance at MF with values between $1{\cdot}10^{-3}$ and 0.1 F·cm^2. Finally, the LF contribution, with a pseudocapacitance $>$ 0.1 F·cm^{-2} at 600 °C, may possibly be attributed to gas phase diffusion limitations of water vapour and oxygen through the porous electrode, but the assignment of MF and LF responses are ambiguous. Overall, electrodes with CuO showed the limiting resistance at low frequencies (LF), whereas for the NiO and Co_3O_4-based electrodes, the LF is smaller and the limiting process is shifted to mid frequencies (MF) (Fig. 4b-c). These results indicate a higher activity for the electrodes with Ni and Co oxides. Also, the higher the content of CuO, the higher the LF resistance contribution, which could be related to mass transport limitations due to electrode shrinkage and/or to lower catalytic activity of CuO for the redox reaction [33,34].

Fig. 5 presents the SEM micrographs of different electrodes after testing. Both electrodes prepared with CuO sintering aid seem to consist of a backbone of BZCY grains decorated by smaller BGLC grains. The BZCY backbone has larger connected grains for the electrode prepared with 5 % CuO versus the one with 2 %, as shown by the fractured surface of the backbone. The electrodes prepared with Co_3O_4 and NiO have a more random microstructural distribution of both phases presented as small grains, contributing to a larger triple-phase boundary area within the electrodes. SEM analysis reveals a good attachment of the electrodes to the electrolyte, and no electrode delamination was detected in any of the cells. The electrode thickness was typically 40–55 μm for the cells with 2 wt% metal oxide as a sintering aid. The electrodes with 5 wt% CuO displayed the lowest thickness, indicating a higher shrinkage and densification for this composition. The estimated porosity fraction of the air electrodes ranged from 38 % to 52 % (Figure S4), which aligns well with the values reported for air electrodes, indicating sufficient porosity to allow efficient gas transport to and from the active reaction sites [5].

In order to study the effect of the electrode thickness on electrochemical performance, an electrode composed of BGLC37/BZCY with 2 wt% CuO (denoted 2Cu 35μm) was coated on a BZCY pellet, and adjusting the printing parameters to reduce its thickness. After thermal treatment, it exhibited a lower thickness of approximately 35 μm (Fig. 6b), and it was electrochemically characterised. Fig. 6a presents the Arrhenius plot of the apparent cell polarisation resistance versus temperature from 600 to 550 °C in humidified air and 1 % O_2 comparing the symmetrical cells 2Cu and 2Cu 35μm. For both atmospheres, the cell with a thinner electrode (2Cu 35μm) systematically displays a lower polarisation resistance, albeit with a modest decrease. In addition, the cell 2Cu 35μm exhibited a lower resistance at HF, as can be observed in Fig. 6b-c, which can be related to the improvement of charge transfer through the electrode due to the lower thickness and/or reduction of isolated active phases in the electrode [35]. Furthermore, the lower electrode thickness facilitates gas transport as can be inferred from the shift in the LF resistance to higher frequencies.

3.3. Fully-assembled tubular proton-ceramic electrolysis cell

The composite electrode BGLC37/BZCY with 2 wt% CuO and 35 μm thickness was applied by dip-coating onto a fully-assembled tubular proton-ceramic electrolysis cell. The assembly consists of an alumina tubular riser, a lower sealing ring, a pre-reduced tube cell, and a sealing cap. The steam electrode was coated on the pre-reduced and sealed Ni/BZCY-supported half-cell and fired at 950 °C for 12 h, resulting in a total active area of 16 cm^2. The electrode thickness is typically 35 μm and presents a similar microstructure as the one observed above. The tubular cell was electrochemically characterised at 600 °C and 4 barg total

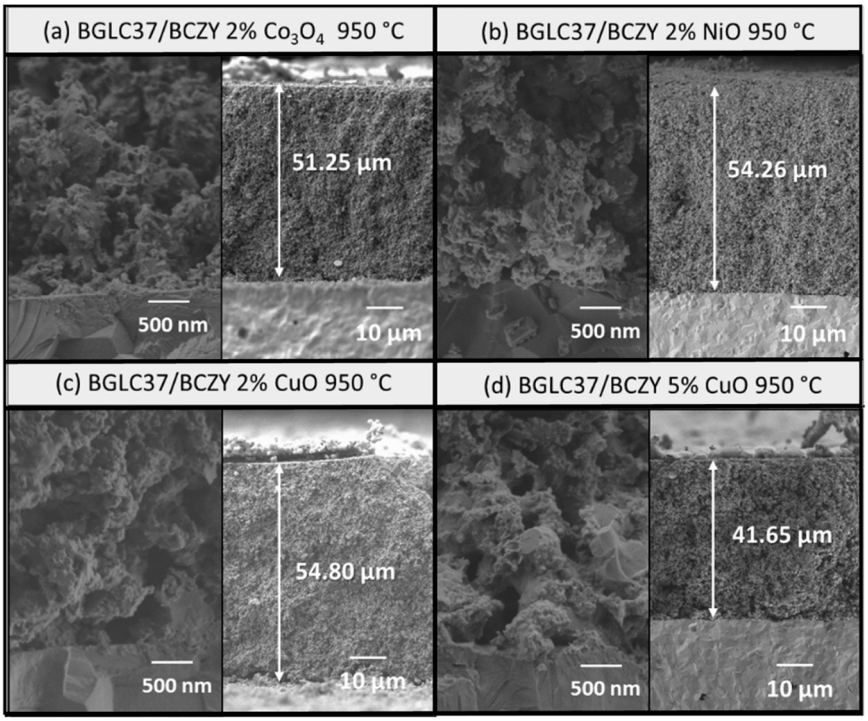

Fig. 5. SEM micrographs of BGLC37/BZCY 2 wt% Co_3O_4 (a), BGLC37/BZCY 2 wt% NiO (b), BGLC37/BZCY 2 wt% CuO (c) and BGLC37/BZCY 5 wt% CuO (d) electrodes after electrochemical testing (broken surface in cross-section view with two different magnifications).

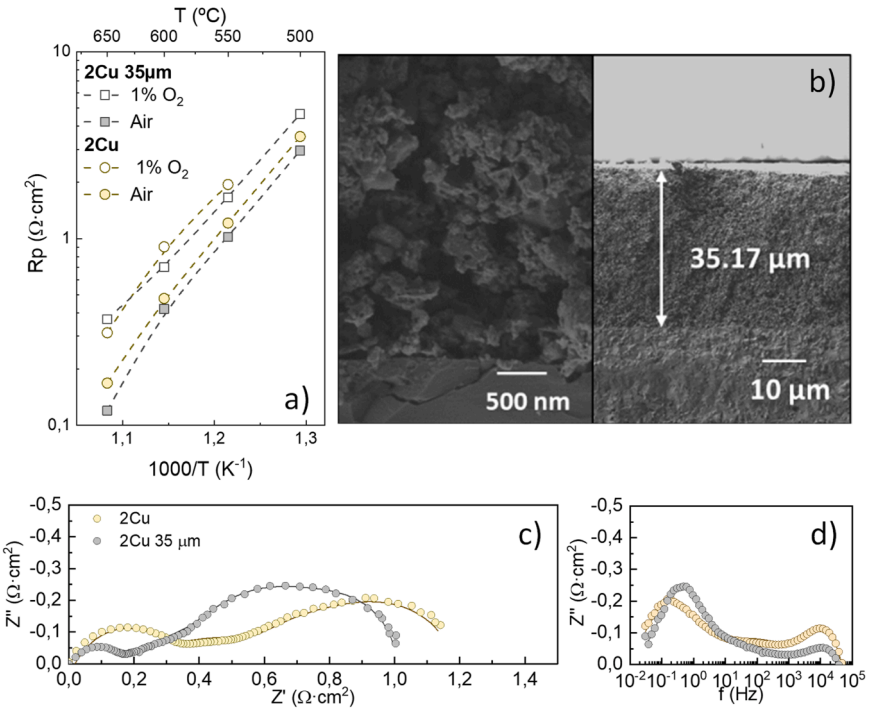

Fig. 6. Total Rp for 2Cu electrodes with two different thicknesses as a function of reciprocal temperature in humidified air and 1 % O_2 (a). Nyquist (b) and Bode (c) plots at 550 °C in wet air of the BGLC37/BZCY with 2 wt% CuO electrodes. Solid lines indicate the fitted equivalent-circuit model.

pressure on both compartments. The steam electrode was fed with 50 % air and 50 % steam, while the hydrogen electrode was swept with 1.5 bar H_2, 0.25 bar H_2O, and 2.25 bar Ar. Impedance data were collected under open-circuit conditions and electrolytic bias (20 and 30 $mAcm^{-2}$), and the corresponding Nyquist spectra are plotted in Fig. 7a.

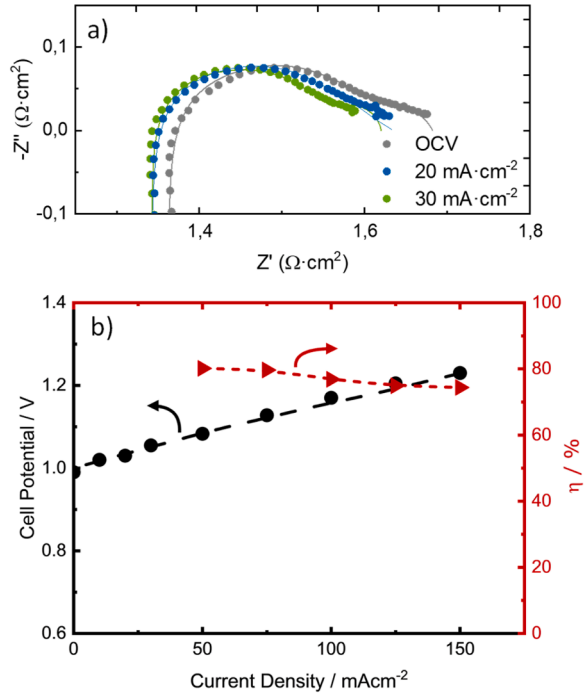

Fig. 7. Nyquist plot at OCV and BIAS (Solid lines indicate the fitted equivalent-circuit model) (a) and IV-response and faradaic efficiency (b) for a fully-assembled tubular electrolysis cell with BZCY-BGLC37 2CuO electrode. Measurements performed at 600 °C and 4 barg (50 % steam, 50 % air on the steam electrode).

The apparent overall polarization resistance (comprising both electrodes) is 0.35 $\Omega \cdot cm^2$ under open-circuit conditions, with a slight activation and reduction of the resistance as the cell is operated in electrolysis mode. These results confirm that the good adhesion and electrode performance obtained for the button cells (<1 cm^2) are successfully transferred to fully-assembled tubular electrolysis cells with larger active areas (16 cm^2).

Fig. 7b displays the IV curve at 600 °C and the corresponding faradaic efficiency of the cell as a function of current density. The faradaic efficiency was calculated by directly measuring the H_2 concentration in the outlet gas stream from the hydrogen electrode compartment. The cell displays open-circuit voltages of 0.99 V (98 % of theoretical value), indicating low electronic and gaseous leakage across the cell when the system is kept idle. The cell presented good performance, allowing operation at 150 $mA \cdot cm^{-2}$ with a voltage of 1.2 V, at faradaic efficiencies of 70–80 %.

The cell was tested in galvanostatic mode at a current density of

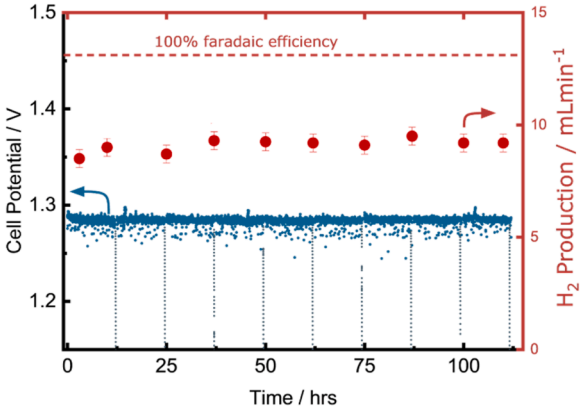

Fig. 8. Stability test of the cell performed at 600 °C in galvanostatic operation (150 mA/cm^2) showing negligible degradation in both cell potential and H_2 production.

150 mA/cm^2 for over 100 hours under a total pressure of 3 bar (Fig. 8). The positrode was exposed to 50 % steam in air, while the negatrode operated with a gas mixture of 10 % steam, 30 % H_2, and 40 % Ar. Negligible degradation was observed in both cell potential and hydrogen production rate over time, confirming the cell robustness due to improved interface adhesion from the sintering aids.

4. Conclusions

The electrode adhesion, microstructure, and electrochemical performance were investigated for ceramic-ceramic steam electrodes based on BGLC37/BZCY to enable the manufacturing of robust large-scale tubular proton-ceramic cells. The effect of different sintering aids, such as Ni, Co, and Cu oxides, on the required firing temperature and sinterability was assessed. The use of sintering aids reduced to 950 °C the temperature of adhesion needed for these composite electrodes. After calcination at 950 °C, the electrodes were successfully attached to the electrolyte with a suitable microstructure, homogeneous distribution of phases, and a high number of interfacial contact points.

Electrochemical impedance spectroscopy on electrolyte-supported button cells with symmetrical configuration revealed that sintering aid addition led to excellent electrochemical performance. Only minor differences in terms of polarisation resistance were observed among the different electrodes. The electrodes with 2 wt% of Ni, Co, and Cu oxides presented the best performance among all the composite electrodes tested. High contents of a sintering aid (5 wt%. of CuO) had a negative effect on the electrode performance, increasing the electrode shrinkage and limiting the transport in the electrode-electrolyte interface of electrodes. Furthermore, the electrode thickness for the composite electrode with 2 wt% of CuO was optimised resulting in an apparent polarisation resistance of 0.4 Ω·cm^2 at 600 °C in wet air.

The sintering procedure was successfully transferred from button cells to large-scale tubular pre-reduced Ni/BZCY-supported half-cells (16 cm^2). A BGLC37/BZCY and 2 wt% CuO steam electrode was applied and sintered at 950 ºC in a fully-assembled tubular electrolysis cell. The steam electrode showed good adhesion, and the sealing interfaces remained undamaged upon sintering. The cell exhibited apparent total polarisation resistances as low as 0.35 Ω·cm^2 (for both electrodes) and faradaic efficiencies of 70–80 % at 600 °C. Those results show the applicability of sintering aids in tailoring the firing temperature of steam electrodes and, therefore, overcoming the mismatch problems that appear during the manufacturing of large-scale proton-ceramic cells.

CRediT authorship contribution statement

Laura Almar: Writing – review & editing, Writing – original draft, Visualization, Validation, Investigation. **Laura Navarrete:** Writing – review & editing, Writing – original draft, Visualization, Validation, Methodology, Investigation, Data curation, Conceptualization. **David Catalán-Martínez:** Writing – review & editing, Writing – original draft, Validation, Investigation, Conceptualization. **Asif Mahmood:** Methodology, Investigation, Conceptualization. **Einar Vøllestad:** Writing – review & editing, Writing – original draft, Validation, Methodology, Investigation, Formal analysis, Conceptualization. **Mateusz Tarach:** Validation, Investigation. **Jose M. Serra:** Writing – review & editing, Writing – original draft, Supervision, Resources, Funding acquisition, Conceptualization. **Truls Norby:** Writing – review & editing, Validation, Funding acquisition. **Marie-Laure Fontaine:** Writing – review & editing, Supervision, Resources, Project administration, Conceptualization. **Sonia Escolástico:** Writing – review & editing, Visualization, Supervision.

Declaration of Competing Interest

The authors declare that they have no known competing financial interests or personal relationships that could have appeared to influence the work reported in this paper.

Acknowledgment

This work is part of the GAMER and WINNER projects that have received funding from the Fuel Cell and Hydrogen 2 Joint Undertaking under Grant Agreement No 779486 and No 101007165. This Joint Undertaking receives support from the European Union's Horizon 2020 Research and Innovation programme, Hydrogen Europe and Hydrogen Europe Research.

Appendix A. Supporting information

Supplementary data associated with this article can be found in the online version at doi:10.1016/j.jeurceramsoc.2024.117162.

References

[1] E. Vøllestad, R. Strandbakke, M. Tarach, D. Catalán-Martínez, M.L. Fontaine, D. Beeaff, D.R. Clark, J.M. Serra, T. Norby, Mixed proton and electron conducting double perovskite anodes for stable and efficient tubular proton ceramic electrolysers, Nat. Mater. 18 (2019) 752–759, https://doi.org/10.1038/s41563-019-0388-2.

[2] S. Choi, T.C. Davenport, S.M. Haile, Protonic ceramic electrochemical cells for hydrogen production and electricity generation: Exceptional reversibility, stability, and demonstrated faradaic efficiency, Energy Environ. Sci. 12 (2019) 206–215, https://doi.org/10.1039/c8ee02865f.

[3] N. Bausá, J.M. Serra, Robust catalytically-activated LSM-BCZY-based composite steam electrodes for proton ceramic electrolysis cells, RSC Adv. 9 (2019) 20677–20686, https://doi.org/10.1039/c9ra04044g.

[4] H. Malerød-Fjeld, D. Clark, I. Yuste-Tirados, R. Zanón, D. Catalán-Martinez, D. Beeaff, S.H. Morejudo, P.K. Vestre, T. Norby, R. Haugsrud, J.M. Serra, C. Kjølseth, Thermo-electrochemical production of compressed hydrogen from methane with near-zero energy loss, Nat. Energy 2 (2017) 923–931, https://doi.org/10.1038/s41560-017-0029-4.

[5] L. Almar, S. Escolástico, L. Navarrete, D. Catalán-Martínez, J. Ara, S. Remiro-Buenamañana, I. Quina, J.M. Serra, Protonic ceramic electrolysis cells (PCECs), Lect. Notes Energy 95 (2023) 245–276, https://doi.org/10.1007/978-3-031-22508-6_9.

[6] WORLD CLASS Innovative novel nanoscale optimized electrodes and electrolytes for electrochemical reactions | Winner | Project | Fact sheet | H2020 | CORDIS | European Commission, (n.d.). ⟨https://cordis.europa.eu/project/id/101007165⟩.

[7] Game changer in high temperature steam electrolysers with novel tubular cells and stacks geometry for pressurized hydrogen production | GAMER | Project | Fact sheet | H2020 | CORDIS | European Commission, (n.d.). ⟨https://cordis.europa.eu/project/id/779486⟩.

[8] W. Sitte, R. Merkle (Eds.), High-Temperature Electrolysis, IOP Publishing, 2023, https://doi.org/10.1088/978-0-7503-3951-3.

[9] S.M. Babiniec, S. Ricote, N.P. Sullivan, Characterization of ionic transport through BaCe0.2 Zr0.7Y0.1O3−δ membranes in galvanic and electrolytic operation, Int. J. Hydrog. Energy 40 (2015) 9278–9286, https://doi.org/10.1016/j.ijhydene.2015.05.162.

[10] S. Ricote, N. Bonanos, H.J. Wang, R. Haugsrud, Conductivity, transport number measurements and hydration thermodynamics of BaCe0.2Zr0.7Y(0.1−ξ)NiξO(3−δ), Solid State Ion.-. 185 (2011) 11–17, https://doi.org/10.1016/j.ssi.2010.12.012.

[11] K.R. Lee, C.J. Tseng, S.C. Jang, J.C. Lin, K.W. Wang, J.K. Chang, T.C. Chen, S. W. Lee, Fabrication of anode-supported thin BCZY electrolyte protonic fuel cells using NiO sintering aid, Int. J. Hydrog. Energy 44 (2019) 23784–23792, https://doi.org/10.1016/J.IJHYDENE.2019.07.097.

[12] A.M. Dayaghi, J.M. Polfus, R. Strandbakke, A. Pokle, L. Almar, S. Escolástico, E. Vøllestad, J.M. Serra, R. Haugsrud, T. Norby, Effects of sintering additives on defect chemistry and hydration of BaZr0.4Ce0.4(Y,Yb)0.2O3−δ proton conducting electrolytes, Solid State Ion.-. 401 (2023) 116355, https://doi.org/10.1016/j.ssi.2023.116355.

[13] Y. Yamazaki, R. Hernandez-Sanchez, S.M. Haile, High total proton conductivity in large-grained yttrium-doped barium zirconate, Chem. Mater. 21 (2009) 2755–2762, https://doi.org/10.1021/CM900208W.

[14] P. Babilo, T. Uda, S.M. Haile, Processing of yttrium-doped barium zirconate for high proton conductivity, J. Mater. Res. 22 (2007) 1322–1330, https://doi.org/10.1557/JMR.2007.0163.

[15] K.Y. Park, Y. Seo, K.B. Kim, S.J. Song, B. Park, J.Y. Park, Enhanced proton conductivity of yttrium-doped barium zirconate with sinterability in protonic ceramic fuel cells, J. Alloy. Compd. 639 (2015) 435–444, https://doi.org/10.1016/J.JALLCOM.2015.03.168.

[16] B. Wang, L. Bi, X.S. Zhao, Exploring the role of NiO as a sintering aid in BaZr0.1Ce0.7Y0.2O3-Δ electrolyte for proton-conducting solid oxide fuel cells, J. Power Sources 399 (2018) 207–214, https://doi.org/10.1016/J.JPOWSOUR.2018.07.087.

[17] A.K. Baral, Y. Tsur, Sintering aid (ZnO) effect on proton transport in BaCe0.35Zr0.5Y0.15O3-δ and electrode phenomena studied by distribution function of relaxation times, J. Am. Ceram. Soc. 102 (2019) 239–250, https://doi.org/10.1111/JACE.15881.

[18] S. Ricote, N. Bonanos, A. Manerbino, N.P. Sullivan, W.G. Coors, Effects of the fabrication process on the grain-boundary resistance in BaZr0.9Y0.1O3-δ, J. Mater. Chem. A Mater. 2 (2014) 16107–16115, https://doi.org/10.1039/C4TA02848A.

[19] E. Vøllestad, M. Schrade, J. Segalini, R. Strandbakke, T. Norby, Relating defect chemistry and electronic transport in the double perovskite Ba1-xGd0.8La0.2+xCo2O6-δ (BGLC), J. Mater. Chem. A Mater. 5 (2017) 15743–15751, https://doi.org/10.1039/c7ta02659e.

[20] R. Strandbakke, V.A. Cherepanov, A.Yu Zuev, D.S. Tsvetkov, C. Argirusis, G. Sourkouni, S. Prünte, T. Norby, Gd- and Pr-based double perovskite cobaltites as oxygen electrodes for proton ceramic fuel cells and electrolyser cells, Solid State Ion.-. 278 (2015) 120–132, https://doi.org/10.1016/J.SSI.2015.05.014.

[21] N. Bausá, C. Solís, R. Strandbakke, J.M. Serra, Development of composite steam electrodes for electrolyzers based on barium zirconate, Solid State Ion.-. 306 (2017) 62–68, https://doi.org/10.1016/j.ssi.2017.03.020.

[22] S.L. Wachowski, I. Szpunar, M.H. Sørby, A. Mielewczyk–Gryń, M. Balaguer, C. Ghica, M.C. Istrate, M. Gazda, A.E. Gunnæs, J.M. Serra, T. Norby, R. Strandbakke, Structure and water uptake in BaLnCo2O6−δ (Ln =La, Pr, Nd, Sm, Gd, Tb and Dy), Acta Mater. 199 (2020) 297–310, https://doi.org/10.1016/j.actamat.2020.08.018.

[23] D. Malyshkin, A. Novikov, I. Ivanov, V. Sereda, D. Tsvetkov, A. Zuev, The origin of triple conductivity and water uptake in layered double perovskites: A case study on lanthanum-substituted GdBaCo2O6−δ, J. Alloy. Compd. 845 (2020) 156309 https://doi.org/10.1016/j.jallcom.2020.156309.

[24] Q. Wang, S. Ricote, M. Chen, Oxygen electrodes for protonic ceramic cells, Electro Acta 446 (2023) 142101, https://doi.org/10.1016/j.electacta.2023.142101.

[25] R. Strandbakke, E. Vøllestad, S.A. Robinson, M.-L. Fontaine, T. Norby, Ba0.5Gd0.8La0.7Co2O6-δ infiltrated in porous BaZr0.7Ce0.2Y0.1O3 backbones as electrode material for proton ceramic electrolytes, J. Electrochem Soc. 164 (2017) F196–F202, https://doi.org/10.1149/2.0141704jes.

[26] R. Strandbakke, D.S. Wragg, M.H. Sørby, M.N. Guzik, A.E. Gunnæs, I. Szpunar, S. L. Wachowski, M. Balaguer, P.A. Carvalho, A. Mielewczyk-Gryń, J.M. Serra, T. Norby, Structural properties of mixed conductor Ba1−xGd1−yLax+yCo2O6−δ, Dalton Trans. 51 (2022) 18667–18677, https://doi.org/10.1039/D2DT02277J.

[27] X. Lu, Y. Chen, Y. Ding, B. Lin, A cobalt-free Sm0.5Sr0.5FeO3−δ–BaZr0.1Ce0.7Y0.2O3−δ composite cathode for proton-conducting solid oxide fuel cells, Int. J. Hydrog. Energy 37 (2012) 8630–8634, https://doi.org/10.1016/j.ijhydene.2012.02.050.

[28] N. Bausá, S. Escolástico, J.M. Serra, Direct CO2 conversion to syngas in a BaCe0.2Zr0.7Y0.1O3- δ-based proton-conducting electrolysis cell, J. CO2 Util. 34 (2019) 231–238, https://doi.org/10.1016/j.jcou.2019.05.037.

[29] B. Fan, J. Yan, W. Shi, A high performance solid oxide fuel cells operating at intermediate temperature with a modified interface between cathode and electrolyte, J. Eur. Ceram. Soc. 30 (2010) 1803–1808, https://doi.org/10.1016/j.jeurceramsoc.2010.01.035.

[30] D. Chen, F. Wang, Z. Shao, Interlayer-free electrodes for IT-SOFCs by applying Co3O4 as sintering aid, Int. J. Hydrog. Energy 37 (2012) 11946–11954, https://doi.org/10.1016/j.ijhydene.2012.05.053.

[31] A. Mielewczyk-Gryń, S. Yang, M. Balaguer, R. Strandbakke, M.H. Sørby, I. Szpunar, A. Witkowska, S. Wachowski, J.M. Serra, A. Navrotsky, M. Gazda, Energetics of formation and stability in high pressure steam of barium lanthanide cobaltite double perovskites, Dalton Trans. 52 (2023) 5771–5779, https://doi.org/10.1039/D2DT03989C.

[32] E. Fabbri, L. Bi, D. Pergolesi, E. Traversa, High-performance composite cathodes with tailored mixed conductivity for intermediate temperature solid oxide fuel cells using proton conducting electrolytes, Energy Environ. Sci. 4 (2011) 4984–4993, https://doi.org/10.1039/C1EE02361F.

[33] S.M. Choi, J.-H. Lee, H.Il Ji, K.J. Yoon, J.-W. Son, B.-K. Kim, H.J. Je, H.-W. Lee, J.-H. Lee, Fabrication and characterization of Ba(Zr0.84Y0.15Cu0.01)O3−δ electrolyte-based protonic ceramic fuel cells, Ceram. Int. 39 (2013) 9605–9611, https://doi.org/10.1016/j.ceramint.2013.05.081.

[34] E.A. Filonova, E.S. Tokareva, N.S. Pikalova, A.I. Vylkov, N.M. Bogdanovich, E. Yu Pikalova, Assessment of prospective cathodes based on (1-x)Ca3Co4O9+ δ-xBaCe0.5Zr0.3Y0.1Yb0.1O3-δ composites for protonic ceramic electrochemical cells, J. Solid State Electrochem. 24 (2020) 1509–1521, https://doi.org/10.1007/s10008-020-04606-1.

[35] L. Navarrete, M. Balaguer, V.B. Vert, J.M. Serra, Tailoring electrocatalytic properties of solid oxide fuel cell composite cathodes based on (La0.8Sr0.2)0.95MnO3+ δ and doped cerias Ce1–xLnxO2–δ (Ln=Gd, La, Er, Pr, Tb and x=0.1–0.2), Fuel Cells 17 (2017) 100–107, https://doi.org/10.1002/fuce.201600133.